In vivo bone response to 3D periodic hydroxyapatite scaffolds assembled by direct ink writing

Joshua L. Simon,[1] Sarah Michna,[2] Jennifer A. Lewis,[2,3] E. Dianne Rekow,[4] Van P. Thompson,[5] James E. Smay,[6] Andrew Yampolsky,[5] J. Russell Parsons,[1] John L. Ricci[5]

[1]*Department of Orthopaedics, University of Medicine and Dentistry of New Jersey, Newark, New Jersey 07103-2714*
[2]*Materials Science and Engineering Department, University of Illinois at Urbana-Champaign, Urbana, Illinois 61801*
[3]*Chemical and Biomolecular Engineering Department, University of Illinois at Urbana-Champaign, Urbana, Illinois 61801*
[4]*Division of Biological Science, Medicine and Surgery, New York University, New York, New York 10010*
[5]*Department of Biomaterials and Biomimetics, New York University, New York, New York 10010*
[6]*Chemical Engineering Department, Oklahoma State University, Stillwater, Oklahoma 74078*

Received 26 February 2006; revised 6 November 2006; accepted 8 February 2007
Published online 8 June 2007 in Wiley InterScience (www.interscience.wiley.com). DOI: 10.1002/jbm.a.31329

Abstract: The *in vivo* bone response of 3D periodic hydroxyapatite (HA) scaffolds is investigated. Two groups of HA scaffolds (11 mm diameter × 3.5 mm thick) are fabricated by direct-write assembly of a concentrated HA ink. The scaffolds consist of cylindrical rods periodically arranged into four quadrants with varying separation distances between rods. In the first group, HA rods (250 μm in diameter) are patterned to create pore channels, whose areal dimensions are 250 × 250 μm^2 in quadrant 1, 250 × 500 μm^2 in quadrants 2 and 4, and 500 × 500 μm^2 in quadrant 3. In the second group, HA rods (400 μm in diameter) are patterned to create pore channels, whose areal dimensions of 500 × 500 μm^2 in quadrant 1, 500 × 750 μm^2 in quadrants 2 and 4, and 750 × 750 μm^2 in quadrant 3. Each group of scaffolds is partially densified by sintering at 1200°C prior to being implanted bilaterally in trephine defects of skeletally mature New Zealand White rabbits. Their tissue response is evaluated at 8 and 16 weeks using micro-computed tomography, histology, and scanning electron microscopy. New trabecular bone is conducted rapidly and efficiently across substantial distances within these patterned 3D HA scaffolds. Our observations suggest that HA rods are first coated with a layer of new bone followed by subsequent scaffold infilling via outward and inward radial growth of the coated regions. Direct-write assembly of 3D periodic scaffolds composed of micro-porous HA rods arrayed to produce macro-pores that are size-matched to trabecular bone may represent an optimal strategy for bone repair and replacement structures. © 2007 Wiley Periodicals, Inc. J Biomed Mater Res 83A: 747–758, 2007

Key words: bone scaffolds; hydroxyapatite; periodic; direct writing; colloidal inks

INTRODUCTION

Hydroxyapatite (HA) scaffolds have been widely investigated as porous bone fillers[1] because of their biocompatibility[2] and osteoconductivity.[3–5] HA scaffolds have been produced by chemical conversion of natural structures such as coral[6,7] and trabecular bone.[8,9] Alternate techniques that aim to mimic naturally occurring architectures have also been reported, including foaming ceramic slurries,[10–12] slip casting sponges,[13] or addition of organic particles (porogens) to ceramic powders.[14,15] Unfortunately, the HA scaffolds produced from each of these approaches possess a broad distribution of randomly connected porosity; hence, elucidating the mechanistic influence of pore size and architecture on tissue response has been difficult.

Solid freeform fabrication (SFF) techniques,[16–38] such as three-dimensional printing (3DP),[27] robocasting,[32–34] fused deposition,[16,26] and stereolithography,[19,28–30] allow the construction of 3D HA scaffolds with controlled architecture and porosity. These techniques rely on computer-aided design to manufacture structures in a predefined pattern with controlled feature size and geometry without the need for subsequent machining. SFF has been employed to directly build structures[16–27] and to create molds that serve as templates for the desired structures.[19,28–31] 3DP has been used to create bone scaffolds with minimum feature sizes on the order of several hundred micrometers.[27] In this technique, binder droplets are ink-jet

Correspondence to: J. L. Ricci; e-mail: john.ricci@nyu.edu or J. A. Lewis; e-mail: jalewis@uiuc.edu

Contract grant sponsor: NASA; contract grant number: NAG8-1922

printed onto a HA powder bed to locally fuse the particles into the desired form. Because of droplet spreading and wetting within the porous bed, 3DP yields HA scaffolds with rough surfaces and limited feature resolution. Alternately, fused deposition[16,26] relies on continuous extrusion of a particle-filled, molten polymer filament to create HA scaffolds with relatively smooth features that are defined by the nozzle size. Finally, 3D HA scaffolds have been created by stereolithography via a lost mold technique.[19,28–30] In this approach, a laser is rastered across a photocurable monomeric resin to create a negative replica of the desired scaffold structure within a polymeric mold. The scaffold is produced by infiltrating the mold with an HA suspension, drying the structure, removing the organic mold by heating to elevated temperatures followed by sintering. Note, HA scaffolds produced by either fused deposition or stereolithography often require lengthy heating cycles to successfully remove organic species without introducing defects.[39]

Michna, Wu, and Lewis[33] recently developed a concentrated HA ink with tailored viscoelastic properties suitable for direct-write assembly of 3D periodic scaffolds with multiscale porosity. In this approach, the ink is continuously extruded in filamentary form to create the desired scaffold structure in a layer-by-layer build sequence.[32] Because the ink contains minimal organic species (ca. 1–2% by volume), the scaffolds can be rapidly heated after drying.[39] By controlling sintering conditions, HA scaffolds were produced with a bimodal pore size distribution, that is, macro-pores that are interconnected between patterned filaments and micro-pores that exist within the partially sintered HA filaments (or rods).

Here, we investigate the *in vivo* bone response to 3D periodic HA scaffolds implanted bilaterally in trephine defects in skeletally mature New Zealand White rabbits. Two groups of HA scaffolds are fabricated with quadrant-specific features by direct-write assembly of concentrated HA inks followed by partial sintering at 1200°C. Their tissue response is evaluated at 8 and 16 weeks using a combination of micro-computed tomography, histology, and scanning electron microscopy to probe the effects of multiscale porosity on bone ingrowth. We show that these HA scaffolds are highly osteoconductive, promoting rapid in growth of new trabecular bone across substantial distances followed by subsequent scaffold infilling via radial growth of the newly coated regions.

MATERIALS AND METHODS

Hydroxyapatite inks

Commercially available HA powder, $Ca_{10}(PO_4)_6(OH)_2$ (Lot # 13310, Reidel-de Haën, Germany) with an average particle diameter of 2.78 μm, as measured by centrifugal photo-sedimentation (Capa-700, Horiba Instruments, Irvine, CA) and a specific surface area of 75.7 m^2/g, as measured by nitrogen adsorption (ASAP 2400 BET, Micrometrics, Norcross, GA) serves as the colloidal phase for scaffold fabrication. The as-received HA powder is calcined at 1100°C for 10 h followed by ball milling for 15 h at 30 rpm to create a powder suitable for ink formulation. The calcined HA powder has an average particle diameter of ~2 μm and a specific surface area of 3.8 m^2/g.

Concentrated HA suspensions (49 vol %) are produced by mixing HA powder and an ammonium polyacrylate solution (Darvan 821A, RT Vanderbilt, Norwalk, CT), which promotes the dispersion of HA particles in deionized water. The optimal dispersant concentration is 0.57 mg disperant/m^2 HA powder. First, the dispersant is added to deionized water and its pH adjusted to 9 by adding an aliquot of a 5*M* NH_4OH solution. The HA powder is then added to this solution in four parts. After each powder addition, the suspension is placed on a paint shaker (Red Devil 5400, Red Devil Equipment Col, Plymouth, MN) for 10 min. A few zirconia grinding media are included to improve mixing. Upon the final addition of HA powder, the suspension is placed on the paint shaker for 20 min. Next, hydroxypropyl methylcellulose (Methocel F4M, Dow Chemical Company, Midland, MI) is added in an amount of 5 mg/mL of solution as a thickening agent along with 1 vol % 1-octanol (Fisher Scientific, Pittsburgh, PA) to prevent foaming. The suspension is again mixed for 15 min on the paint shaker. The pH is readjusted to 9 by the addition of a 1*M* HNO_3 solution, followed by an additional 10 min on the paint shaker. Finally, the suspension is gelled by adding 2*M* $Ca(NO_3)_2$ solution in increments of 0.05 mL to produce a concentrated HA ink with the appropriate viscoelastic properties required for direct-write assembly of the 3D scaffolds.[32,33] The HA ink is placed on the paint shaker for 10 min after adding separate aliquots of gelling agent and 20 min after the final addition.

Scaffold design and assembly

HA scaffolds (11 mm diameter × 3.5 mm thick) with 3D periodic quadrant architectures are fabricated by direct-write assembly of concentrated colloidal HA ink. Each scaffold consists of cylindrical HA rods periodically arranged in four quadrants with a specified separation distance between the rods (Fig. 1), creating pore channels for bone in growth. Two groups of specimens are created. The first group contains 250 μm HA rods patterned with macro-pore channel dimensions of 250 × 250 μm^2 (DW250S) in quadrant 1, 250 × 500 μm^2 (DW250M) in quadrants 2 and 4, and 500 × 500 μm^2 (DW250L) in quadrant 3, whereas the second group contains 400 μm HA rods patterned with macro-pore channel dimensions of 500 × 500 μm^2 (DW400S) in quadrant 1, 500 × 750 μm^2 (DW400M) in quadrants 2 and 4, and 750 × 750 μm^2 (DW400L) in quadrant 3. The void contents associated with the interconnected macro-pores in each quadrant design are provided in Table I.

Our direct-write process employs a 3-axis, motion-control robotic stage to move a vertically held deposition noz-

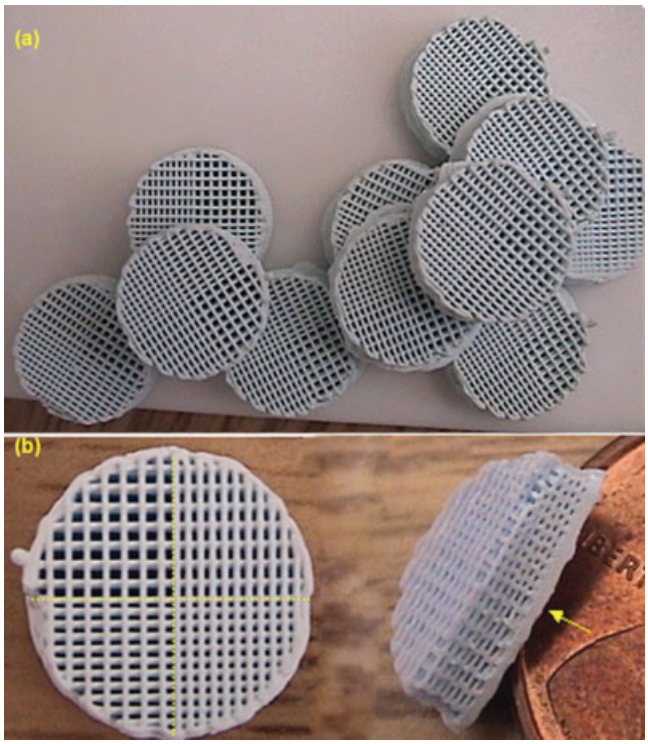

Figure 1. Optical micrographs of (a) HA scaffolds patterned with the DW250 quadrant design and (b) top and cross-sectional views of a representative DW250 scaffold illustrating the four distinct periodic arrays and their solid capping layer, respectively.

zle in a predefined pattern parallel to the horizontal *x-y* plane (JL2000, Sandia National Laboratories, Albuquerque, NM). The ink is dispensed at a constant volumetric flow rate by a syringe pump attached to the deposition nozzle. The print pattern is designed using custom software (RoboCAD 3.0, 3D Inks, Stillwater, OK). Using an optimized ink, we measured the spatial reproducibility of 100 μm rods patterned with a center-to-center separation distance of 200 μm in the *x-y* plane to be 188 ± 4.6 μm.[36] Here, each scaffold is printed in a layer-by-layer build sequence at a deposition speed of 3 mm/s using a cylindrical deposition nozzle (D = 250 or 400 μm). Each layer contained HA rods (diameter = D) patterned with different values of the minimum separation (gap) distance between rods on each half of the circular cross-section. Once a given layer is constructed, the nozzle is translated up a distance ($\sim 0.9D$) and another layer is deposited by rotating the desired pattern by 90°. This process is repeated until the entire 3D scaffold has been printed. Both groups of HA scaffolds (final diameter of 11 mm after partial densification) are fabricated with a solid cap-

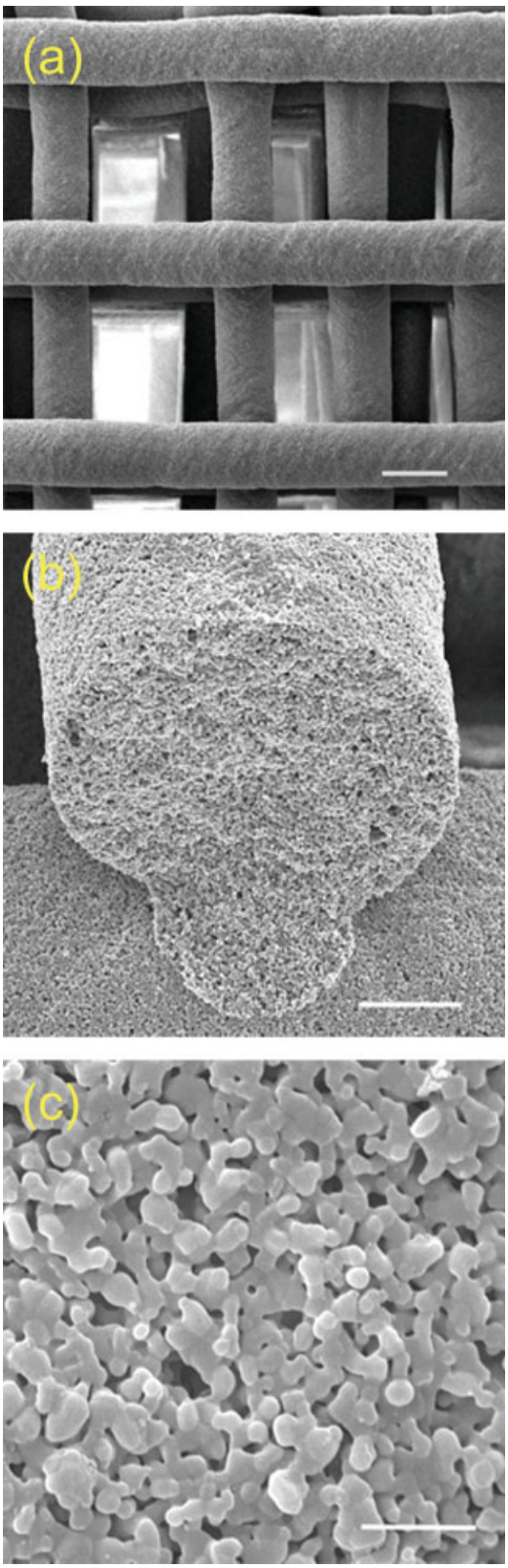

Figure 2. Scanning electron micrographs of (a) HA scaffold with DW250 quadrant design showing the 500 × 500 μm^2 spacing between HA rods (left side) and the 250 × 500 μm^2 spacing between HA rods (right side) regions (scale bar = 250 μm), (b) fracture surface showing the connections between the two HA rods in adjacent layers (scale bar = 50 μm), and (c) higher magnification view of HA rod surface showing an interconnected (partially sintered) network of HA particles (roughly 2 μm in diameter) with intervening fine-scale porosity (~1 μm in characteristic size[33]) (scale bar = 10 μm).

TABLE I
HA Scaffold Design Specifications

Designation	Rod Size (μm)	Rod Spacing (μm)	Void Volume (mm^3)	% Void Volume
DW250S	250	250/250	20.7	56
DW250M	250	250/500	23.9	64
DW250L	250	500/500	27.1	71
DW400S	400	500/500	22.7	61
DW400M	400	500/750	24.7	65
DW400L	400	750/750	26.7	70

ping layer (no gap between rods) to minimize soft-tissue infiltration from the overlying soft tissue (see Fig. 1). Each scaffold is produced within a low viscosity oil reservoir to prevent drying during the assembly process.[32] After assembly is complete, the oil is drained and each scaffold is allowed to dry uniformly in air. The HA scaffolds are then heat-treated at 400°C for 1 h, 900°C for 2 h, and, finally, 1200°C for 2 h to allow partial densification. A total of 20 scaffolds are produced within each group.

Scaffold characterization

The dimensions of the HA rods and interconnected, large pore channels are determined by image analysis (Bioquant Image Analysis Software, Version 3.50.6, R&M Biometrics, Nashville, TN). One scaffold from each group is also scanned using micro-computed tomography (Micro CT, MS-8, GE Medical Systems, London, Ontario, Canada) to determine the characteristic rod and pore channel dimensions prior to the implant procedure.

Animal procedures

Bilateral 11 mm diameter trephine defects are created in the calvaria of skeletally mature New Zealand White rabbits weighting between 3.5 and 4.0 kg, following procedures approved by the institutional animal care and use committee. Two defects are created in each animal, one on each side of the saggital suture. Each animal received two scaffolds, one from the first group (250 μm HA rods) and the other from the second group (400 μm HA rods). A total of 16 implants (8 from each group) are implanted in 8 rabbits for analysis at 8 weeks. Another 16 (8 from each group) are implanted in 8 rabbits for analysis at 16 weeks.

Morphine (0.02 mg/kg) analgesic and enrofloxicin (5 mg/kg) antibiotic is administered a few minutes prior to surgery. The animals are anesthetized by intramuscular injections of acepromazine (0.5 mg/kg), glycopyrolate (0.5 mg/kg), xylazine (5 mg/kg), and ketamine (35 mg/kg). The surgical site is shaved and cleaned with poviodine. A fentanyl (50 μg/h) patch for pain management is applied to the skin in a location away from the surgical site. The initial surgical incision is made parallel to the sagittal suture through both skin and periosteum and the layers are retracted to expose the left and right parietal bones. Trephine defects are created in both the left and right parietal bones using a hand powered T-bar drill taking care not to disturb the dura below the bone.

Prior to insertion, each scaffold is sterilized with gamma irradiation at a dose of 25 kGY (Sterigenics, Somerset, NJ). At implantation, each scaffold is soaked in 1 mL of fresh blood for 5–10 min, drawn from a major artery in the ear to ensure nutrient-containing hematoma formation and increased initial protein adsorption within the scaffold. After soaking, the scaffolds are inserted into the defects, the periosteum closed, and the skin closed as described previously.[40,41]

Animals are housed in stainless steel hutches and kept at 19–25°C in ventilated air at ~55% relative humidity with food and water ad lib. They received treatment with enrofloxicin (5 mg/kg) for 5 days postoperatively. The fentanyl patches are removed after 3 days.

Implant analysis

Animals are sacrificed at 8 and 16 weeks and specimens of the scaffold and surrounding bone are extracted as described previously.[42] Specimens are stored in 10% neutral buffered formalin prior to being examined by micro-computed tomography (Micro CT, MS-8, GE Medical Systems, London, Ontario, Canada) at a resolution of 20 μm using a shutter speed of 3000 ms, with a 1 × 1 bin size. Four hundred micrographs are taken at incremental angles within each scan and software rendered with 2 × 2 x-bin and y-bin sizes to create ~20-μm × 20-μm × 20-μm voxel size 3D images. The 3D images are viewed using MicroView software (version 1.1, build 0015, GE Medical Systems, Fairfield, CT) for analysis of bone response. A total volume of interest (VOI) measuring 2 mm × 3 mm × 3 mm (18 mm^3) is superimposed on the 3D reconstruction image for each quadrant within each scaffold. Within this volume, a manual segmentation method is used to measure; (1) combined bone and scaffold volume, (2) bone volume, and (3) by subtraction, soft tissue volume. The total volume of all components is verified to match the VOI.

Upon completion of all micro-CT scans, samples from each group at each time point are embedded in polymethyl methacrylate according to standard hard tissue histology protocols. Coronal plane sections are stained with Van Gieson's Picrofucn and Stevenel's Blue to determine tissue response using optical microscopy. In this procedure, calcified bone stains bright red with an intensity that varies depending bone maturity. Digital photographs of the sections are then taken. Using standard histological techniques, cell types and morphologies are determined. Signs of inflammation, if found, are catalogued. Sections are examined for gross morphology and bone ingrowth pathways.

Scanning electron microscopic analysis is carried out on the remaining block specimens used for histological analysis, to evaluate bone morphology, bone response to the scaffolds, extent of mineralization, and condition of the scaffolds, in backscattered electron imaging (BEI) mode and X-ray microprobe (XRM) analysis mode. This is conducted on a Hitachi S3500 scanning electron microscope (source) equipped with a GW Electronics (Norcross, GA) BEI detector system and a PGT Imix XRM system equipped with a PRISM light element detector (Princeton Gamma Tech, Princeton, NJ).

RESULTS

Scaffold structure

HA scaffolds fabricated by direct-write assembly consist of 3D periodic arrays of cylindrical HA rods orthogonally arranged in successive layers in a quadrant design, as shown in Figure 1. Several scaffolds from the first group (250 μm HA rods) are shown in Figure 1(a), with corresponding optical images of their top surface and cross-section provided in Figure 1(b). The cross-sectional view reveals the presence of a solid base layer along with several periodic layers comprised of macro-pore channels with varying dimensions formed by patterning the HA rods at different separation distances in the *x*- and *y*-directions. The higher magnification image, shown in Figure 2(a), verifies that the HA rods are arranged so that the minimum and maximum separation distances between adjacent rods are 250 μm and 500 μm, respectively. Each scaffold consists of well-defined quadrants with in-plane (*x*-*y*) macro-pore channel dimensions 250 × 250 μm^2 (DW250S), 250 × 500 μm^2 (DW250M), 500 × 250 μm^2 (also DW250M), and 500 × 500 μm^2 (DW250L). Similarly, images acquired on the HA scaffolds comprised of 400 μm rods (not shown) reveal the presence of quadrants with minimum and maximum separation distances between rods of 500 μm and 750 μm, respectively, yielding quadrants with in-plane (*x*-*y*) pore channel dimensions of 500 × 500 μm^2 (DW400S), 500 × 750 μm^2 (DW400M), 750 × 500 μm^2 (also DW400M), and 750 × 750 μm^2 (DW400L). Note, for each set of scaffolds, the macro-pore channel spacing in the *z*-direction is $\sim 0.9D$, where *D* is the HA rod diameter.

The fracture surface of a representative scaffold (DW250) reveals the micro-porous nature of the HA rods after partial densification, as shown in Figure 2(b,c). Well-bonded interfaces form at the junctions between HA rods in adjacent layers [see Fig. 2(b)]. At higher magnification [Fig. 2(c)], one can observe the presence of individual HA particles that have partially sintered together to yield an interpenetrating network comprised of both solid and micro-porous features. Figure 2 clearly demonstrates that these scaffolds possess a bimodal pore size distribution with macro-pores forming between the HA rods [Fig. 2(a)] and micro-pores residing within individual HA rods. The HA rods increased from ~49 to 70% of theoretical density during sintering and possess a characteristic pore size of ~1 mm, as determined by mercury intrusion porosimetry.[33] It should be noted that the total volumes associated with each pore population can be controlled through a combination of direct-write assembly and different sintering conditions.[33]

Bone ingrowth

The rabbit trephine model involves the creation of 11-mm diameter parietal bone defects that represent near-critical size defects. In general, bone response to the scaffolds was excellent. Bone healing and ingrowth are observed in all implanted HA scaffolds after 8- and 16-weeks, as shown in Figures 3 and 4, respectively. Bone healing progresses by rapid ingrowth of new (trabecular) bone from the periphery of the defect into the scaffold along the HA rods. Most of the new bone is observed to originate from the periosteal and endosteal surfaces of the bone adjacent to the defect, with the most extensive growth originating from the periosteal surface and conducted inward near the solid capping layer (see Figs. 3 and 4). Higher magnification views of the scaffold cross-sections show that individual HA rods are coated with new (trabecular) bone, which thickens radially over time [see Figs. 3(c) and 4(c)]. There are no significant instances of inflammation in tissues surrounding or within the scaffold, as shown in Figure 5(a,b) for representative scaffolds after 8 and 16 weeks, respectively. New trabecular bone at the growth front consists of numerous small trabeculae. As the bone matures, it is observed to remodel to a more mature structure, consisting of smaller numbers of larger, lamellar trabeculae. Soft tissue, marrow, and vascular elements are observed to form in this maturing bone (see Fig. 5). Bone near the periphery of the defect was more dense and mature than bone toward the center of the scaffold (see Figs. 3 and 4). The extent and rate of bone formation are observed to be consistent among defects, albeit with regional variations in the amount and organization of bone and soft tissue observed within different defects.

Quantitative evaluation of the bone and soft tissue volumes within the implanted HA scaffolds reveals that the overall amounts of bone ingrowth into all scaffolds at 8 and 16 weeks are comparable, consistent, and very extensive. The extent of bone ingrowth into the six distinct quadrant designs is reported in Figure 6(a). The actual volumes ranged from 6.4 to 7.5mm^3 at 8 weeks to 6.5 to 9.1mm^3 at 16 weeks, where the total volume analyzed is 18 mm^3 in each

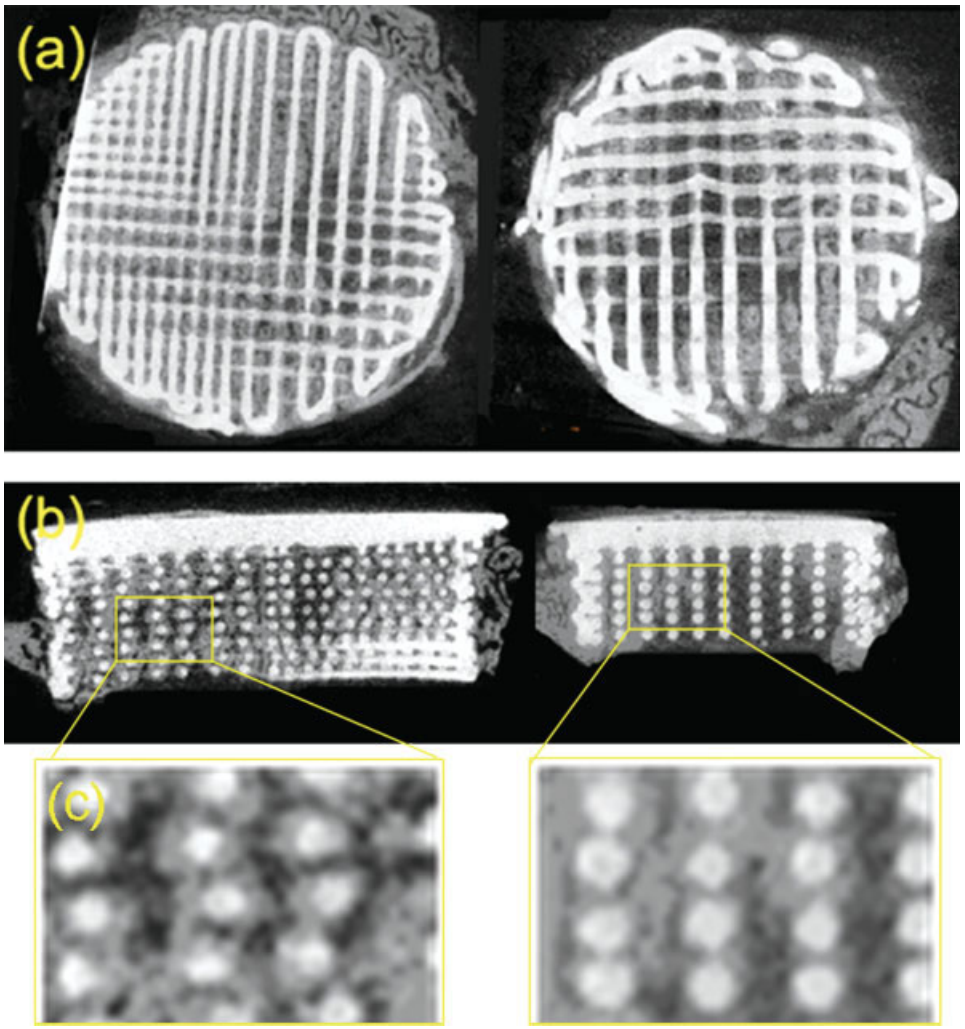

Figure 3. Planar microCT radiographs of the implanted HA scaffolds in the (a) sagittal plane at 8 weeks for DW250 (left radiograph) and DW400 (right radiograph), (b) coronal plane at 8 weeks for DW250 (left radiograph) and DW400 (right radiograph), and (c) corresponding higher magnification views of the regions highlighted in (b).

case. However, when normalized by available macro-pore volume within each quadrant, the values indicate a trend toward increased bone ingrowth in quadrants with smaller macro-pore channels [see Fig. 6(b)]. These normalized volumetric values ranged from 63.5 to 86.7% at 8 weeks to 81.4 to 95.5% at 16 weeks. Correspondingly, the soft tissue volumes are the lowest in the quadrants with the closest spacing between HA rods (i.e., lowest macro-pore volumes).

At both 8 and 16 weeks, bone is observed to (1) attach directly to the surfaces of the HA rods indicating osteoconduction, (2) grow inward along the struts and crossover from one rod to another, and (3) reach the center of the scaffold, as shown in Figures 3–5. Conduction of bone from one HA rod to another is shown in Figure 7(a). In this case, the bone bridging is very symmetrical. The bone is normal in appearance, and by 16 weeks much of the bone is mature and lamellar in structure, as evidenced by rows of organized osteoblasts [Fig. 7(b)]. In some areas, more cellular (and less organized) bone is observed, suggesting active bone formation. Both of these features are seen in different regions of Figure 7. Bone cell response to the implanted scaffolds is characterized by direct bone cell contact at the interface between bone mineral and HA rods in many areas [Fig. 7(b)]. In many cases, these bone cells are observed to send cell processes directly into the pores of the HA matrix. These cells are of normal size and configuration and are not suggestive of any pathological processes. There is excellent compatibility between the HA matrix, the bone cells, and the mineralized bone matrix.

Bone attachment is quite extensive and appears to penetrate deeply into the micro-pores within individual HA rods (Fig. 7). Some of the micro-porous HA rods contain considerable amounts of what is believed to be reprecipitated HA, as highlighted by the higher magnification views of several key features shown in Figure 7. Images of the interface between the micro-porous HA scaffold and soft tissue [Fig.

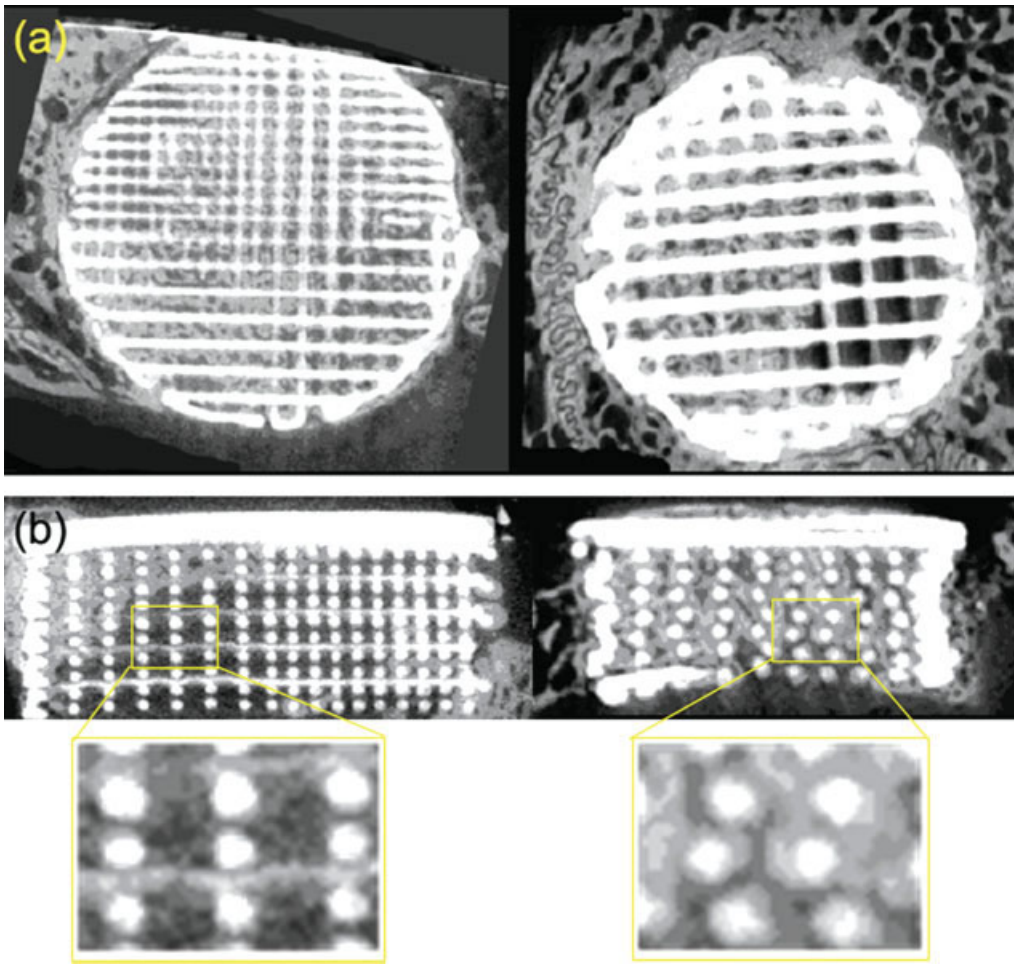

Figure 4. Planar microCT radiographs of the implanted HA scaffolds in the (a) sagittal plane at 16 weeks for DW250 (left radiograph) and DW400 (right radiograph), (b) coronal plane at 16 weeks for DW250 (left radiograph) and DW400 (right radiograph), and (c) corresponding higher magnification views of the regions highlighted in (b).

8(a,b)] or bone [Fig. 8(c,d)] show dramatic differences when acquired in back-scattered electron imaging mode. A significant calcium signal from this region is only detected in the latter case. The material imaged within the micro-porous HA rods is darker than the surrounding sintered HA, suggesting that it is less dense. There are no observed areas of extensive bone resorption other than those seen during normal remodeling. Some these regions (small dark features with uneven borders) are seen in Figure 7(b). How-

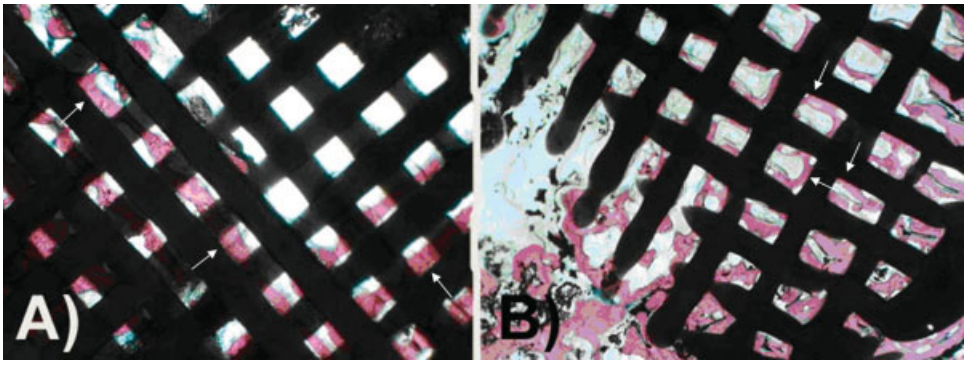

Figure 5. Optical micrographs of a representative section of a DW400 implant after (a) 8 weeks and (b) 16 weeks showing typical patterns of bone and soft tissue organization. Bone trabeculae are organized in patterns indicating that they are being conducted along the HA struts of the scaffolds. [Arrows highlight the conduction of uninterrupted trabeculae for considerable distances in (a), and the crossover of trabeculae from one HA rod to another in (b). The HA rod diameter in each image is $\sim$400 μm.]

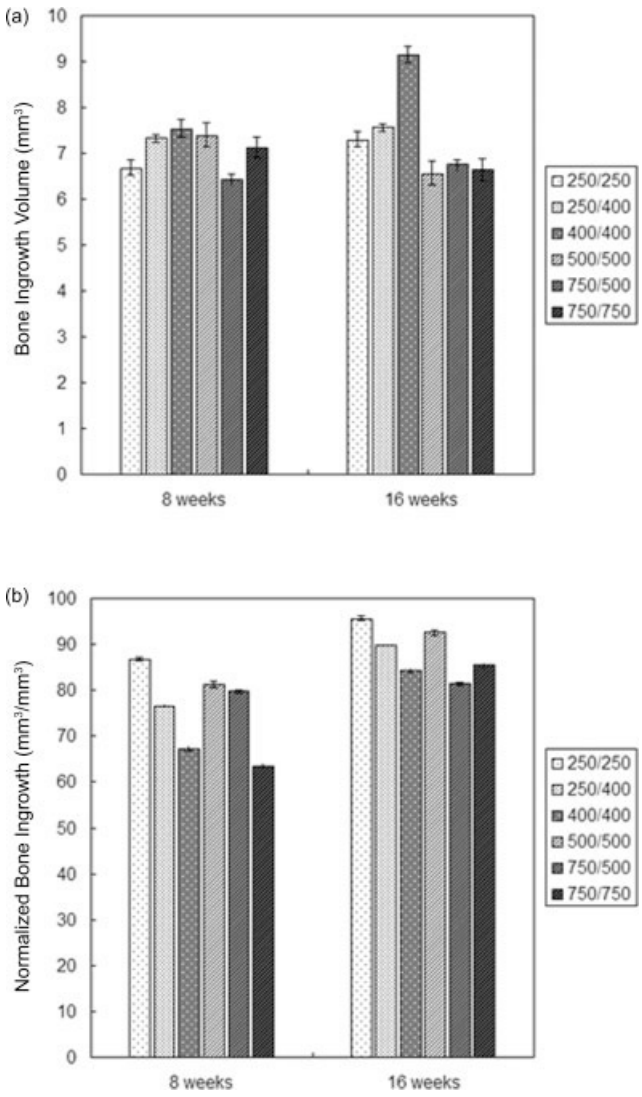

Figure 6. Plots of bone ingrowth into the HA scaffolds with varying quadrant designs: (a) total volume of bone ingrowth and (b) normalized volumetric bone ingrowth.

ever, there is no direct evidence of osteoclastic resorption of the HA. Some cracking of these specimens is also observed [see Fig. 7(a)]. Polymerization shrinkage induces some cracking, however it is notable that the cracking separates significant areas within the HA rods, but only where attached bone has penetrated into these features. This observation provides further evidence that bone mineralization occurs within the micro-porous HA rods; absent this, cracking is expected to occur closer to or along the bone-HA interface.

DISCUSSION

Direct-write assembly of concentrated colloidal inks allows excellent control over the structural features of 3D HA scaffolds at multiple length scales, including the HA rod dimensions, the intervening macro-pore sizes between rods, and the surface roughness and micro-porosity within individual HA rods. The original hypothesis of this work was that the effects of pore size, level of macro-porosity, and rod size could be elucidated by systematically varying these parameters using direct-write assembled scaffolds. However, all the HA rod sizes and macro-pore channel spacings in this study yielded consistent and extensive bone ingrowth across significant distances with full penetration of bone to the scaffold center after 8 weeks. Two unexpected findings emerge from our observations: (1) there appears to be a direct relationship between the sizes of ingrowing bone trabeculae and that of HA rods within these scaffolds and (2) the micro-porous nature of the HA rod appears to promote bone ingrowth within such features.

Human bone trabeculae are reported to be 100–250 μm in diameter, depending on the age and condition of the subject.[43] The bone trabeculae observed in this study are consistent with that size range, and there is often a one-to-one relationship between the characteristic rod size and the bone trabeculae conducted along its surface. The HA rods are often observed to conduct uninterrupted trabeculae along their lengths for considerable distances, as highlighted by arrows in Figure 5(a). The significant ingrowth distances crossed by these combinations of rod sizes and trabeculae suggest that the size match between the two may represent an effective and efficient strategy for design of bone repair scaffolds.

Micro-CT analysis of bone and soft tissue ingrowth suggests that all scaffolds in this study conducted bone to the center of the defect by 8 weeks, and that the bone conduction was consistent and extensive. The percentages of bone ingrowth as a function of available volume are routinely high at 8 and 16 weeks; in the 63.5–95.5% range. Although there is some indication that the scaffolds with closer HA rod spacings filled with slightly more bone as a function of available volume, this is apparently at the expense of soft tissue ingrowth, which is extremely low in the DW250S and DW400S specimens. While these scaffolds varied significantly in their available void volume (see Table I), bone ingrowth appears to be largely independent of this parameter. Bone ingrowth also appears to be independent of available surface area, since a rough estimate for these scaffolds yields significant differences in the surface area between the DW250 and DW400 scaffolds. Since bone ingrowth was largely independent of this parameter, we hypothesize that the bone does not form a layer of consistent thickness on the HA rods (or struts). For similar amounts of bone to form on both scaffolds, bone must have a formed thicker layer on the DW400 scaffold relative to the DW250 scaffold. The electron

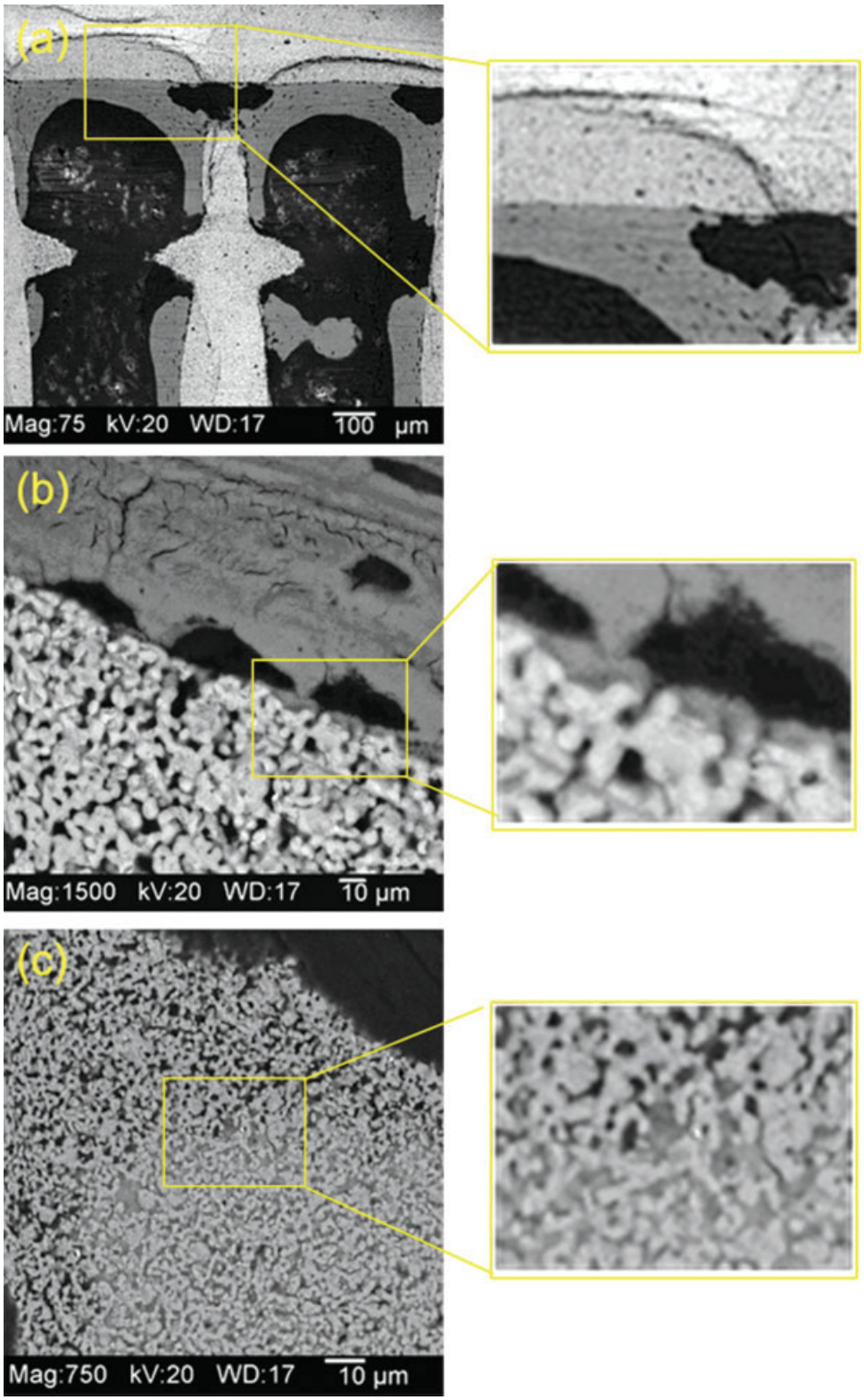

Figure 7. SEM images (acquired in back-scattered electron mode) of (a) cross-sectional view of ingrowing bone and the HA scaffold, (b) cross-sectional view of a localized interfacial region, and (c) cross-section view of bone mineralization deep within the microporous regions of an individual HA rod. Corresponding high magnification views of the regions highlighted in (a–c) are provided alongside these images.

micrographs and micro-CT images suggest that bone forms a coating on the struts and then grows radially, thickening to fill available space (Figs. 3–5). At some earlier time period there may have been a relationship between scaffold surface area and bone conduction, but by 8 and 16 weeks this bone has remodeled to fill

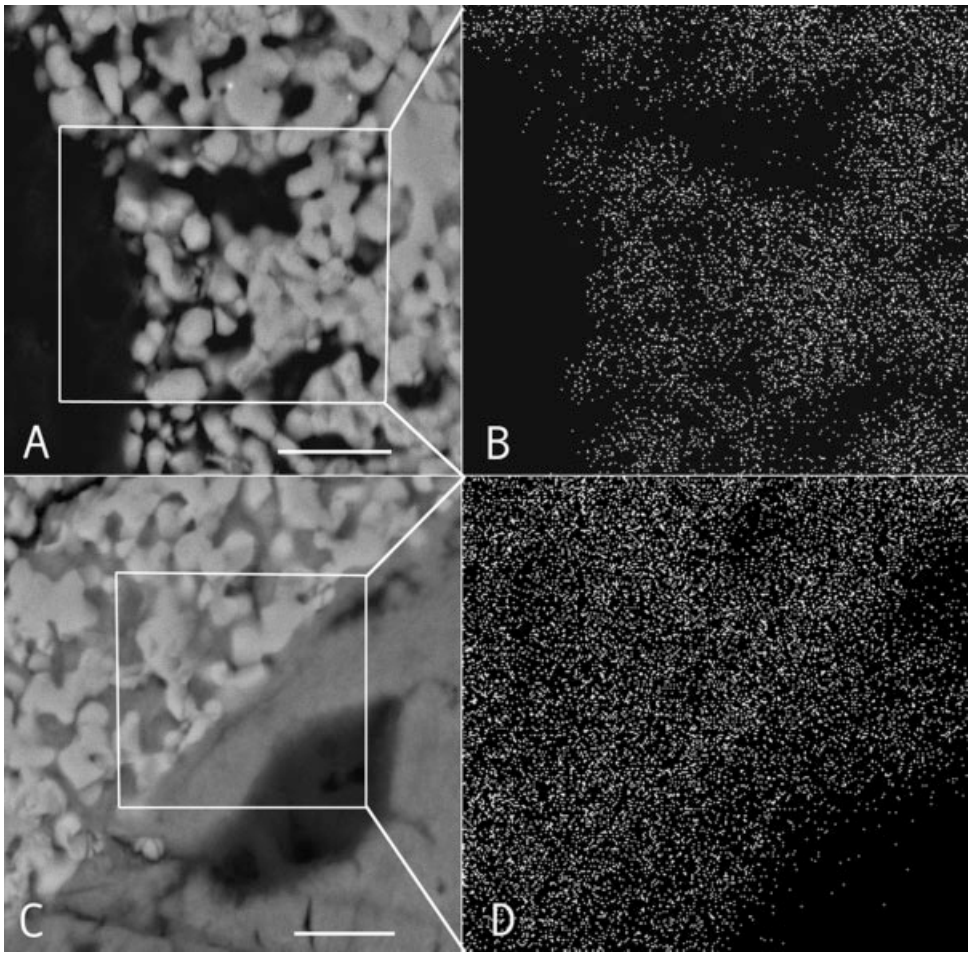

Figure 8. BEI photomicrographs (A and C) and corresponding calcium elemental maps (B and D) of the highlighted areas, showing the interfaces between the micro-porous HA and soft tissue (A and B) or bone (C and D). The surface micro-pores do not yield a calcium signal at the soft tissue interface, whereas a significant calcium signal arises at the bone interface suggesting that the micro-pores are filled with mineral of a density similar to the adjacent bone, but lower than that of the ceramic HA [scale bars = 10 μm].

available space, with the limiting factor being the presence of enough soft tissue to permit blood vessel access, providing adequate blood supply for the bone within the scaffolds.

Mineralization patterns and cellular response to these 3D periodic HA scaffolds also provide some valuable insights. Cell response to these scaffolds, specifically the observation of cells directly attached to the HA scaffolds and sending cell processes into their micro-porous regions, suggest that the cells may have approached these features in much the same way they approach local bone matrix. This unexpected finding is likely related to the patterns of mineralization observed in the HA scaffold material. The mineral observed in the HA matrix, which we believe to be a calcium phosphate of lower density than sintered HA, but comparable to bone mineral, is observed to exist throughout the scaffold struts. Based on the continuity of the internal mineral, surface mineral, and bone matrix mineral observed in Figures 7 and 8, we believe that all three are intimately related. In related work on nearly identical HA scaffolds, Dellinger, Eurell, and Jamison[34] found that scaffolds implanted in the metacarpal and metatarsal bones of goats stained darkly with toluidine blue in the internal regions of the micro-porous HA rods, while those that were not implanted did not. They reported that the dark blue stained regions resembled the color of woven bone, and suggested that the stained material within the rods could be components of extracellular matrix (ECM) secreted by nearby bone cells, byproducts of ECM production that diffused into the scaffold from adjacent bone, or other cellular products that reacted with the scaffold leading to a change in staining characteristics. Taken together, the observations made on 3D periodic HA scaffolds strongly suggest that micro-porosity may play a valuable, though unexpected role, in bone repair.

CONCLUSIONS

This study demonstrates that osteoconductive 3D periodic HA scaffolds with bimodal porosity can be assembled by direct writing. Bone ingrowth into such scaffolds was extensive at both 8 and 16 weeks. Further, the results suggest that the use of HA rods with dimensions similar to that of ingrowing trabecular bone may be an effective method for rapid and efficient conduction of new bone across significant distances in these osteoconductive scaffolds. The apparent presence of precipitated mineral in the scaffolds adjacent to bone mineral suggests an effective combination of scaffold design and cellular mechanisms that result in a continuous mineralized matrix throughout the microporous HA and adjacent bone. The use of direct-write fabrication, with its ability to produce 3D HA scaffolds composed of structural elements that possess multiscale porosity that mimic the microstructure of natural bone, may represent an optimal strategy for the fabrication of bone repair and replacement structures.

We thank the Dana Center of New York University for providing time on their MicroCT apparatus. Special thanks go to Tithi Dutta Roy, Chris Sabatino, and Gregory Gebauer for their surgical assistance. Animal studies were supported through funding from the New Jersey Center for Science and Technology. The authors gratefully acknowledge J. Cesarano (Sandia National Laboratories, Albuquerque, NM) who designed and built the robotic deposition stage.

References

1. Chiroff RT, White EW, Weber KN, Roy DM. Tissue ingrowth of Replamineform implants. J Biomed Mater Res 1975;9:29–45.
2. de Groot K. Bioceramics consisting of calcium phosphate salts. Biomaterials 1980;1:47–50.
3. Chang BS, Lee CK, Hong KS, et al. Osteoconduction at porous hydroxyapatite with various pore configurations. Biomaterials 2000;21:1291–1298.
4. Gauthier O, Bouler JM, Aguado E, Pilet P, Daculsi G. Macroporous biphasic calcium phosphate ceramics: Influence of macropore diameter and macroporosity percentage on bone ingrowth. Biomaterials 1998;19:133–139.
5. Lemperle SM, Calhoun CJ, Curran RW, Holmes RE. Bony healing of large cranial and mandibular defects protected from soft-tissue interposition: A comparative study of spontaneous bone regeneration, osteoconduction, and cancellous autografting in dogs. Plast Reconstr Surg 1998;101:660–672.
6. Roy DM, Linnehan SK. Hydroxyapatite formed from coral skeletal carbonate by hydrothermal exchange. Nature 1974; 247:220–222.
7. White R, White E, Web J. Replamineform: A new process for prepariing prous ceramic, metal, and polymer prosthetic materials. Science 1972;176:922–924.
8. Lin FH, Liao CJ, Chen KS, Sun JS, Lin CY. Preparation of betaTCP/HAP biphasic ceramics with natural bone structure by heating bovine cancellous bone with the addition of (NH(4))(2)HPO(4). J Biomed Mater Res 2000;51:157–163.
9. Tancred DC, McCormack BA, Carr AJ. A synthetic bone implant macroscopically identical to cancellous bone. Biomaterials 1998;19:2303–2311.
10. Rejda BV, Peelen JG, de Groot K. Tri-calcium phosphate as a bone substitute. J Bioeng 1977;1:93–97.
11. Sepulveda P, Binner JG, Rogero SO, Higa OZ, Bressiani JC. Production of porous hydroxyapatite by the gel-casting of foams and cytotoxic evaluation. J Biomed Mater Res 2000;50: 27–34.
12. Tamai N, Myoui A, Tomita T, et al. Novel hydroxyapatite ceramics with an interconnective porous structure exhibit superior osteoconduction in vivo. J Biomed Mater Res 2002; 59:110–117.
13. Woyansky J, Scott C, Minnear W. Processing of porous ceramics. MAm Ceram Soc Bull 1992;71:1674–1682.
14. Bouler JM, Trecant M, Delecrin J, Royer J, Passuti N, Daculsi G. Macroporous biphasic calcium phosphate ceramics: Influence of five synthesis parameters on compressive strength. J Biomed Mater Res 1996;32:603–609.
15. Tsuruga E, Takita H, Itoh H, Wakisaka Y, Kuboki Y. Pore size of porous hydroxyapatite as the cell-substratum controls BMP-induced osteogenesis. J Biochem (Tokyo) 1997;121:317–324.
16. Gomes de Sousa FC, Evans, JRG. Sintered hydroxyapatite latticework for bone substitute. J Am Ceram Soc 2003;86:517–519.
17. Cheah CM, Chua CK, Leong KF, Cheong CH, Naing MW. Automatic algorithm for generating complex polyhedral scaffold structures for tissue engineering. Tissue Eng 2004;10: 595–610.
18. Chua CK, Leong KF, Tan KH, Wiria FE, Cheah CM. Development of tissue scaffolds using selective laser sintering of polyvinyl alcohol/hydroxyapatite biocomposite for craniofacial and joint defects. J Mater Sci Mater Med 2004;15:1113–1121.
19. Cooke MN, Fisher JP, Dean D, Rimnac C, Mikos AG. Use of stereolithography to manufacture critical-sized 3D biodegradable scaffolds for bone ingrowth. J Biomed Mater Res B 2003;64:65–69.
20. Hutmacher DW. Scaffold design and fabrication technologies for engineering tissues–State of the art and future perspectives. J Biomater Sci Polym Ed 2001;12:107–124.
21. Hutmacher DW, Sittinger M, Risbud MV. Scaffold-based tissue engineering: Rationale for computer-aided design and solid free-form fabrication systems. Trends Biotechnol 2004;22:354–362.
22. Sherwood JK, Riley SL, Palazzolo R, et al. A three-dimensional osteochondral composite scaffold for articular cartilage repair. Biomaterials 2002;23:4739–4751.
23. Tan KH, Chua CK, Leong KF, et al. Scaffold development using selective laser sintering of polyetheretherketone-hydroxyapatite biocomposite blends. Biomaterials 2003;24: 3115–3123.
24. Yang S, Leong KF, Du Z, Chua CK. The design of scaffolds for use in tissue engineering. II. Rapid prototyping techniques. Tissue Eng 2002;8:1–11.
25. Yeong WY, Chua CK, Leong KF, Chandrasekaran M. Rapid prototyping in tissue engineering: Challenges and potential. Trends Biotechnol 2004;22:643–652.
26. Zein I, Hutmacher DW, Tan KC, Teoh SH. Fused deposition modeling of novel scaffold architectures for tissue engineering applications. Biomaterials 2002;23:1169–1185.
27. Zeltinger J, Sherwood JK, Graham DA, Mueller R, Griffith LG. Effect of pore size and void fraction on cellular adhesion, proliferation, and matrix deposition. Tissue Eng 2001;7:557–572.
28. Chu TM, Hollister SJ, Halloran JW, Feinberg SE, Orton DG. Manufacturing and characterization of 3D hydroxyapatite bone tissue engineering scaffolds. Ann N Y Acad Sci 2002; 961:114–117.

29. Chu TM, Orton DG, Hollister SJ, Feinberg SE, Halloran JW. Mechanical and in vivo performance of hydroxyapatite implants with controlled architectures. Biomaterials 2002;23: 1283–1293.
30. Levy RA, Chu TM, Halloran JW, Feinberg SE, Hollister S. CT-generated porous hydroxyapatite orbital floor prosthesis as a prototype bioimplant. AJNR Am J Neuroradiol 1997;18: 1522–1525.
31. Wilson CE, de Bruijn JD, van Blitterswijk CA, Verbout AJ, Dhert WJ. Design and fabrication of standardized hydroxyapatite scaffolds with a defined macro-architecture by rapid prototyping for bone-tissue-engineering research. J Biomed Mater Res A 2004;68:123–132.
32. Smay JE, Cesarano J, Lewis JA. Colloidal inks for directed assembly of 3D periodic structures. Langmuir 2002;18:5429–5437.
33. Michna S, Wu W, Lewis JA. Concentrated hydroxyapatite inks for direct-write assembly of 3D periodic scaffolds. Biomaterials 2005;26:5632–5639.
34. Dellinger JG, Eurell JAC, Jamison RD. Bone response to 3D periodic hydroxyapatite scaffolds with and without tailored microporosity to deliver bone morphogenetic protein 2 J. Biomed Mater Res A 2005;76:366–37.
35. Borah B, Gross GJ, Dufresne TE, et al. Three-dimensional microimaging (MRmI and mCT), finite element modeling, and rapid prototyping provide unique insights into bone architecture in osteoporosis. Anat Rec (New Ana) 2001;265: 101–110.
36. Li Q, Lewis J. Nanoparticle inks for directed assembly of 3D periodic structures. Adv Mater 2003;15:1639–1643.
37. Therriault D, White S, Lewis JA. Chaotic mixing in 3D microvascular networks fabricated by direct-write assembly. Nature Mater 2003;2:265–271.
38. Gratson GM, Xu M, Lewis J. Direct writing of three dimensional webs. Nature 2004;428:386.
39. Lewis JA, Cima MJ. Diffusivities of dialkyl phthalataes in plasticized poly(vinyl butyral): Impact on binder thermolysis. J Am Ceram Soc 1990;73:2702–2797.
40. Damien, CJ, Parsons, JR, Benedict, JJ, Weisman, DS. Investigation of a hydroxyapatite and calcium sulfate composite supplemented with an osteoinductive factor. J Biomed Mater Res 1990;24:639–654.
41. Damien CJ, Ricci JL, Christel P, Alexander H, Patat JL. Formation of a calcium phosphate-rich layer on absorbable calcium carbonate bone graft substitutes. Calcif Tissue Int 1994; 55:151–158.
42. Simon JL, Dutta Roy T, Parsons JR, Rekow ED, Thompson VP, Kemnitzer J, Ricci JL. Engineered cellular response to scaffold architecture in a rabbit trephine defect. J Biomed Mater Res A 2003;66:275–282.
43. Li SH, De Wijn JR, Layrolle P, de Groot K. Synthesis of macroporous hydroxyapatite scaffolds for bone tissue engineering. J Biomed Mater Res 2002;61:109–120.